

# Towards Better Adversarial Purification via Adversarial Denoising Diffusion Training

Yiming Liu<sup>\*1</sup> Kezhao Liu<sup>\*1</sup> Yao Xiao<sup>1</sup> Ziyi Dong<sup>1</sup> Xiaogang Xu<sup>2</sup> Pengxu Wei<sup>1</sup> Liang Lin<sup>1</sup>

## Abstract

Recently, diffusion-based purification (DBP) has emerged as a promising approach for defending against adversarial attacks. However, previous studies have used questionable methods to evaluate the robustness of DBP models, their explanations of DBP robustness also lack experimental support. We re-examine DBP robustness using precise gradient, and discuss the impact of stochasticity on DBP robustness. To better explain DBP robustness, we assess DBP robustness under a novel attack setting, Deterministic White-box, and pinpoint stochasticity as the main factor in DBP robustness. Our results suggest that DBP models rely on stochasticity to evade the most effective attack direction, rather than directly countering adversarial perturbations. To improve the robustness of DBP models, we propose Adversarial Denoising Diffusion Training (ADDT). This technique uses Classifier-Guided Perturbation Optimization (CGPO) to generate adversarial perturbation through guidance from a pre-trained classifier, and uses Rank-Based Gaussian Mapping (RBGM) to convert adversarial perturbation into a normal Gaussian distribution. Empirical results show that ADDT improves the robustness of DBP models. Further experiments confirm that ADDT equips DBP models with the ability to directly counter adversarial perturbations.

## 1. Introduction

Deep learning has achieved remarkable success in various domains, including computer vision (He et al., 2016), natural language processing (OpenAI, 2023), and speech recognition (Radford et al., 2022). In this flourishing landscape, however, the persistent specter of adversarial attacks casts a shadow over the reliability of these neural models. Ad-

<sup>\*</sup>Equal contribution <sup>1</sup>Sun Yat-Sen University, Guangzhou, China <sup>2</sup>Zhejiang University, Hangzhou, China. Correspondence to: Pengxu Wei <weipx3@mail.sysu.edu.cn>.

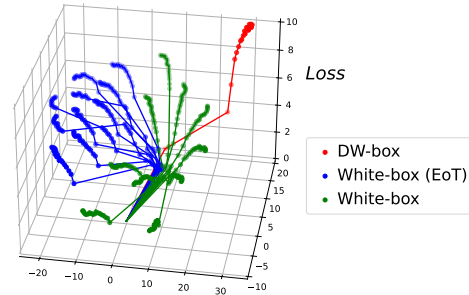


Figure 1: Visualization of attack trajectories under different evaluation settings: Deterministic White-box (DW-box) attack trajectory shows a consistent, targeted increase, while standard White-box attack trajectories are erratic. White-box (EoT) attacks are more focused, but deviate significantly from the Deterministic White-box attack trajectory (higher loss is less robust).

versarial attacks for a vision model involve injecting imperceptible perturbations into input images to trick models into producing false outputs with high confidence (Goodfellow et al., 2015; Szegedy et al., 2014). This inspired a large amount of research on adversarial defense (Zhang et al., 2019; Samangouei et al., 2018; Shafahi et al., 2019; Wang et al., 2023).

Recently, diffusion-based purification (DBP) (Nie et al., 2022) has emerged as a promising approach. It utilizes off-the-shelf diffusion models and can counter various adversarial attacks. However, the robustness evaluation of DBP models in previous studies is questionable, their explanations of DBP robustness also lacks experimental support. Previous work often relies on approximations in gradient computations (Athalye et al., 2018; Wang et al., 2022), and the widely used evaluation framework AutoAttack also shows questionable results when evaluating DBP robustness (Nie et al., 2022). To effectively evaluate DBP robustness, we adopt a comprehensive evaluation method that incorporates Expectation over Transformation (EoT) (Athalye et al., 2018) to address model stochasticity and uses precise gradient calculations. We discuss the poor performance of AutoAttack in evaluating DBP robustness, and propose the use of the Projected Gradient Descent (PGD) attack (Madry et al., 2018) in DBP evaluation.

Traditionally, the robustness of DBP methods has been attributed solely to the forward diffusion process, which reduces the distribution gap between clean and adversarial images by adding Gaussian noise (Wang et al., 2022; Nie et al., 2022). We challenge this view and argue that the robustness of DBP methods stems from the combined stochasticity in both the diffusion forward and reverse processes. To test this hypothesis, we propose to evaluate DBP methods under a novel Deterministic White-box setting, where the attacker knows not only the model parameters, but also all stochastic noise used in the evaluations. This setting makes the model completely deterministic for the attacker. Our evaluation highlights stochasticity in both the forward and reverse processes as a key factor in DBP robustness. It also suggests that diffusion models may inherently lack the ability to directly counter adversarial perturbations like AT-trained models, and instead rely on stochasticity to evade the most effective attack directions, as illustrated in Figure 1.

To improve the robustness of DBP methods against adversarial perturbations, we propose **Adversarial Denoising Diffusion Training** (ADDT). Our approach starts with **Rank-Based Gaussian Mapping** (RBGM), which makes adversarial perturbations compatible with the diffusion framework. Building on this, we generate adversarial perturbations using **Classifier-Guided Perturbation Optimization** (CGPO) and train the model to counter these perturbations.

Our main contributions are as follows:

- We re-examine the robustness of diffusion-based purification (DBP) with a precise gradient, and discuss the impact of DBP stochasticity.
- We evaluate DBP robustness under a new attack setting, Deterministic White-box and identify stochasticity as the main factor of DBP robustness.
- We develop **Adversarial Denoising Diffusion Training**, which equips DBP models with the ability to directly counter adversarial perturbations. Our empirical studies confirm its effectiveness.

## 2. Related Work

**Adversarial Training.** First introduced by Madry et al. (Madry et al., 2018), adversarial training (AT) has nearly become the de facto standard for strengthening neural networks (Gowal et al., 2020; Rebuffi et al., 2021; Athalye et al., 2018). Recent advances in AT have harnessed the generative power of diffusion models to augment training datasets and prevent AT from overfitting (Gowal et al., 2021; Wang et al., 2023). However, the application of AT to DBP methods has not been thoroughly explored.

**Adversarial Purification.** Adversarial purification uses generative models to purify adversarial noise before evaluation. Adversarial purification traditionally uses generative

models such as GANs (Samangouei et al., 2018) or autoregressive models (Song et al., 2018). Recently, adversarial purification using diffusion models (Song & Ermon, 2019; Ho et al., 2020; Song et al., 2020a), termed diffusion-based purification (DBP), has shown encouraging results (Nie et al., 2022; Wang et al., 2022; Wu et al., 2022; Xiao et al., 2022). These works attribute the robustness of DBP models to the wash-out effect of the Gaussian noise added in the forward diffusion process. DiffPure (Nie et al., 2022) suggests that the KL divergence between clean and adversarial image distributions decreases after forward diffusion. (Gao et al., 2022) suggests that the forward diffusion process reduces model invariance and contributes to robustness, while the reverse process restores invariance and degrades robustness. However, these works are evaluated against unreliable attacks. Since diffusion models rely on iterative denoising, some works use mathematical approximations of gradients to reduce memory requirements (Athalye et al., 2018) or bypass the diffusion process during backpropagation (Wang et al., 2022). What’s more, even the performance of AutoAttack (Croce & Hein, 2020), the most widely used evaluation method is questionable. AutoAttack offers a *Rand* version to evaluate stochastic models, however, Nie *et al.* report that when evaluating DBP robustness, this *Rand* version is some times, less effective than the *Standard* version (Nie et al., 2022). The explanation for the robustness of the DBP models also lacks experimental support.

## 3. Preliminaries

**Adversarial Training.** Adversarial training aims to create a robust model by including adversarial samples during training (Madry et al., 2018). This approach can be formulated as a min-max problem, where we first generate adversarial samples (the maximization) and then adjust parameters to resist these adversarial samples (the minimization). Mathematically, this is represented as:

$$\min_{\theta} \mathbb{E}_{(x,y) \sim \mathcal{D}} [\max_{\delta \in B} L(f(\theta, x + \delta), y)] \quad (1)$$

In this equation,  $L$  is the loss function,  $f$  is the classifier,  $(x, y) \sim \mathcal{D}$  denotes sampling training data from distribution  $\mathcal{D}$ , and  $B$  defines the set of permissible perturbation  $\delta$ .

**Diffusion Models.** Denoising Diffusion Probabilistic Models (DDPM) (Ho et al., 2020) and Denoising Diffusion Implicit Models (DDIM) (Song et al., 2020a) simulate a gradual transformation in which noise is added to images and then removed to restore the original image. The forward process can be represented as:

$$x_t = \sqrt{\bar{\alpha}_t} x_0 + \sqrt{1 - \bar{\alpha}_t} \epsilon, \quad \epsilon \sim \mathcal{N}(0, I) \quad (2)$$

where  $x_0$  is the original image and  $x_t$  is the noisy image.  $\bar{\alpha}_t$  is the cumulative noise level at step  $t$  ( $1 < t \leq T$ , where  $T$

is the number of diffusion training steps). The model optimizes the parameters  $\theta$  by minimizing the distance between the actual and predicted noise:

$$\theta^* = \arg \min_{\theta} \mathbb{E}_{\mathbf{x}_0, t, \epsilon} [\|\epsilon - \epsilon_{\theta}(\sqrt{\alpha_t}\mathbf{x}_0 + \sqrt{1 - \alpha_t}\epsilon, t)\|_2^2] \quad (3)$$

$\epsilon_{\theta}$  is the model’s noise prediction, with  $\epsilon_{\theta}$ , we can predict  $\hat{\mathbf{x}}_0$  in a single step:

$$\hat{\mathbf{x}}_0 = (\mathbf{x}_t - \sqrt{1 - \alpha_t}\epsilon_{\theta^*}(\mathbf{x}_t, t)) / \sqrt{\alpha_t} \quad (4)$$

where  $\hat{\mathbf{x}}_0$  is the recovered image. DDPM typically takes an iterative approach to restore the image, removing a small amount of Gaussian noise at a time:

$$\hat{\mathbf{x}}_{t-1} = \left( \mathbf{x}_t - \frac{\beta_t}{\sqrt{1 - \alpha_t}} \epsilon_{\theta^*}(\mathbf{x}_t, t) \right) / \sqrt{1 - \beta_t} + \sqrt{\beta_t} \epsilon \quad (5)$$

where  $\beta_t$  is the noise level at step  $t$ ,  $\hat{\mathbf{x}}_{t-1}$  is the recovered image in step  $t - 1$ ,  $\epsilon$  is sampled from  $\mathcal{N}(0, \mathbf{I})$ . DDIM proposes to speed up the denoising process by skipping certain intermediate steps. Recent work suggests that DDPM may also benefit from a similar approach (Nichol & Dhariwal, 2021). Score SDEs (Song et al., 2020b) give a score function view of DDPM and further lead to the derivations of DDPM++ (VPSDE) and EDM (Karras et al., 2022).

**Diffusion-Based Purification (DBP).** DBP (Nie et al., 2022; Wang et al., 2022; Wu et al., 2022) uses diffusion models to remove adversarial noise from images. Instead of using a complete diffusion process between the clean image and pure Gaussian noise (between  $t = 0$  and  $t = T$ ), they first diffuse  $\mathbf{x}_0$  to a predefined timestep  $t = t^* (t^* < T)$  via Equation (2), and recover the image  $\hat{\mathbf{x}}_0$  via the reverse diffusion process in Equation (5).

## 4. Stochasticity-Driven Robustness

Previous research has provided unreliable robustness evaluations and lacks experimental support for explaining the robustness of Diffusion-Based Purification (DBP) models. To address these issues, we introduce a more rigorous evaluation framework in Section 4.1. Our re-evaluation shows that stochasticity has a significant impact on DBP robustness. In Section 4.2, we then investigate the robustness of DBP models in a novel deterministic white-box setting and confirm that stochasticity is the key factor influencing DBP robustness. Moreover, in Section 4.3 we identify a potential limitation: unlike adversarial training (AT) models, diffusion models may inherently lack mechanisms to directly counter adversarial perturbations. Instead, DBP models rely primarily on stochastic elements to circumvent the most effective attack vectors.

Table 1: Evaluation of state-of-the-art DBP methods, EoT significantly influenced the evaluation of model robustness.

	DiffPure	GDMP (MSE)	DP <sub>DDPM</sub>	DP <sub>DDIM</sub>
Clean	89.26	91.80	85.94	88.38
PGD20-EoT1	69.04	53.13	60.25	54.59
PGD20-EoT10	55.96	40.97	47.27	42.19

### 4.1. Revisiting Diffusion-Based Purification Robustness

As discussed in Section 2, previous studies evaluate DBP robustness based on inaccurate gradients and questionable evaluation methods, making their result unreliable. To address this, we propose a re-evaluation of DBP models. Evaluating DBP robustness poses two challenges: the introduction of Gaussian noise during evaluation, which can render adversarial perturbations generated during the attack ineffective in the evaluation, and the iterative denoising steps during evaluation, which result in high memory requirements during backpropagation. To address these challenges, we use the Expectation over Transformation (EoT) method (Athalye et al., 2018) to average gradients across different attacks, and use the precise gradient of the complete diffusion-classification pipeline, while saving memory using gradient checkpointing (Chen et al., 2016). Also, instead of AutoAttack, we used the traditional PGD attack for evaluation<sup>1</sup>.

We re-evaluated several DBP methods, including DiffPure, GDMP, and adaptations of DDPM and DDIM within the DiffPure framework (DP<sub>DDPM</sub> and DP<sub>DDIM</sub>). GDMP uses DDPM models for purification, while DiffPure used VPSDE (DDPM++) models which is more resource-intensive. Tests were performed on CIFAR-10 dataset using a WideResNet-28-10 (Zagoruyko & Komodakis, 2016) classifier against a 20-step PGD  $l_{\infty}$  attack with 10 EoT iterations (EoT10) and no EoT (EoT1). For a detailed experimental setup, see Section 6.1. Further discussion about EoT and the choice of EoT iterations can be found in Appendix A.

As shown in Table 1, regardless of the use of EoT, our evaluation yielded an accuracy below the originally claimed 70.64% for DiffPure and 90.10% for GDMP. This underscores the necessity of using the exact gradient of the entire diffusion-classification pipeline to evaluate the robustness of DBP models. In addition, all models showed lower robustness in the EoT evaluation, highlighting the importance of considering model stochasticity in DBP evaluations.

### 4.2. Stochasticity as the Main Factor of DBP Robustness

The robustness of DBP models has traditionally been attributed solely to the forward diffusion process, which adds

<sup>1</sup>We discover a bug in the *Rand* of AutoAttack that caused it to overestimate the robustness of DBP. After fixing this, as discussed in Appendix I, AutoAttack gives similar results to PGD attacks, but at a much higher computational cost.

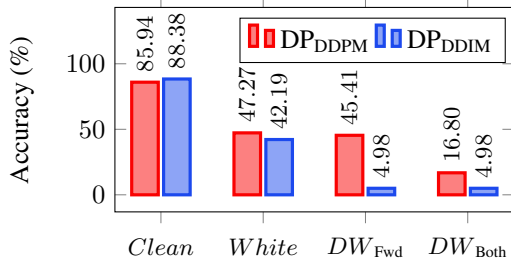


Figure 2: DP<sub>DDPM</sub> and DP<sub>DDIM</sub> robustness under different setting. Both models lost most of their robustness only when attacker know all stochastic elements (DW<sub>Both</sub>-box for DP<sub>DDPM</sub> and DW<sub>Fwd</sub>-box for DP<sub>DDIM</sub>).

Gaussian noise to the clean and adversarial images, thus reducing their distribution gap (Wang et al., 2022; Nie et al., 2022). On the contrary, we argue that the robustness of DBP models is a result of the combined stochasticity in both the forward and reverse processes. To explore this, we introduce a new attack setting, Deterministic White-box, which gives the attacker complete knowledge for evaluating models that contain stochastic elements. In the conventional White-box setting, the attacker only knows the model parameters and must resort to resampling the stochastic noise at random. In the Deterministic White-box setting, however, the attacker has full knowledge of not only the model parameters but also the stochastic noise used during the evaluation phase. This makes the DBP process deterministic to the attacker, allowing for more accurate perturbation generation. It’s important to note that the Deterministic White-box setting is hypothetical. It’s designed to analyze DBP model mechanics, not for real-world use.

We evaluate the robustness of DP<sub>DDPM</sub> and DP<sub>DDIM</sub> under different attack settings. DP<sub>DDPM</sub> includes Gaussian noise in both the forward and reverse processes, while DP<sub>DDIM</sub> includes Gaussian noise only in the forward process. We distinguish attacks based on their knowledge of the stochastic elements: no knowledge (White-box), full knowledge of the forward process (DW<sub>Fwd</sub>-box), or both processes (DW<sub>Both</sub>-box). Under the traditional view, which attributes DBP robustness to the forward diffusion process, attacking DDPM and DDIM in the DW<sub>Fwd</sub>-box setting should yield similar results. However, in our view, which emphasizes stochasticity in both processes, attacking DP<sub>DDIM</sub> in the DW<sub>Fwd</sub>-box setting should yield similar results to DP<sub>DDPM</sub> in the DW<sub>Both</sub>-box setting, when both models become fully deterministic for the attacker.

The results are shown in Figure 6, DDPM remains robust in the DW<sub>Fwd</sub>-box setting, while DDIM loses most of its robustness. Their different behavior challenges the traditional explanation that only the forward process affects the robustness of DBP models. However, in the DW<sub>Both</sub>-box setting, both DDPM and DDIM are not robust. This confirms our

explanation that DBP robustness is due to stochasticity in both the forward and reverse processes<sup>2</sup>.

Previous research has questioned whether stochasticity can improve robustness, arguing that it can produce obfuscated gradients that give a false sense of security (Athalye et al., 2018). The concern is that there is still a vulnerable direction that works for all stochastic noise, but the stochasticity prevents the attacker from finding it. To investigate this, we implemented DW<sub>Semi</sub>-box, a semi-stochastic setting that restricts the stochastic elements to a limited set of options. Our results show that stochasticity can indeed improve robustness, even when the attacker have full knowledge of the possible stochastic elements options. For a detailed analysis of our results, see Appendix B.

### 4.3. Shortages in Stochasticity-Driven Robustness

The robustness of DBP models may not be due to an inherent ability to counter adversarial perturbations like AT-trained models. Instead, we argue that these models rely on stochasticity to evade the most effective attack direction. Note that this idea doesn’t challenge the robustness of DBP models, but offers a new perspective that complements previous work (Xiao et al., 2022; Carlini et al., 2022). To support our argument, we analyze attack trajectories under different attack settings. We use t-SNE to plot the attack trajectories on the  $xy$  plane, with the loss plotted on the  $z$ -axis. We examined three attack settings, PGD20-EoT10/PGD20-EoT1 attack under White-box setting (denoted as White-box (EoT) and White-box) and PGD20-EoT1 attack under Deterministic White-box setting (denoted as DW-box). The results are shown in Figure 1, our analysis showed that while the attacks trajectories in both the White-box and Deterministic White-box setting are scattered due to the stochasticity of the DBP models, the Deterministic White-box attacks show a more directional and steady increase. Although the White-box (EoT) attack trajectories appear more focused compared to the White-box attacks, they still deviate from the most effective path identified in the Deterministic White-box attack. This shows that the DBP models cannot inherently counter adversarial perturbations, but rely on stochasticity to evade the most effective attack direction.

From a loss landscape perspective, we argue that the loss landscape of DBP models is not inherently smooth. To illustrate this, we focus on a single White-box (EoT) attack and a Deterministic White-box attack trajectory, place them in a 2D space, and visualize them on the loss landscape (Li et al., 2018) (Kim et al., 2021). The results are shown in Figure 3. For experimental details, see Appendix C. As shown on the left side of the figure 3, there is a significant increase in loss in the Deterministic White-box attack direc-

<sup>2</sup>The potential to further improve robustness by increasing the stochasticity of the model is discussed in Appendix G.

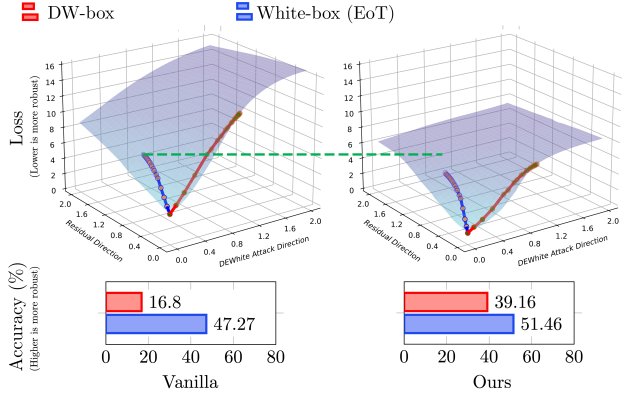


Figure 3: Visualization of the attack trajectory under different settings. The Deterministic White-box attack is more effective, while the White-box (EoT) attack deviates from the Deterministic White-box attack trajectory, indicating a less efficient attack.

tion, indicating that the loss landscape of DBP models is not inherently flat. This is different from AT-trained models, which show only a small change in loss in the adversarial direction (Shafahi et al., 2019). It is noteworthy that the loss changes less dramatically in the direction of the White-box (EoT) attack. We argue that this occurs because the White-box (EoT) attack fails to find the most effective direction, as shown in Figure 1.

## 5. Adversarial Denoising Diffusion Training

To improve the robustness of DBP models against adversarial perturbations, we propose **Adversarial Denoising Diffusion Training** (ADDT). ADDT uses an iterative two-step approach: the **Classifier-Guided Perturbation Optimization** (CGPO) step generates adversarial perturbations, while the training step trains on these perturbations and updates diffusion model parameters. We illustrate this in Figure 4 and further detailed with pseudocode in Appendix E. With ADDT, we can efficiently fine-tune clean models to directly counter adversarial perturbations, we briefly discussed the efficiency in Appendix K.

In Section 5.1, we discuss how to make adversarial perturbations compatible with the diffusion framework using **Rank-Based Gaussian Mapping** (RBGM). We then present ADDT in Section 5.2. Our approach generates adversarial perturbations under the guidance of a classifier, a process we term **Classifier-Guided Perturbation Optimization** (CGPO), and trains the diffusion model to withstand these perturbations.

### 5.1. Rank-Based Gaussian Mapping

We propose to strengthen diffusion models by incorporating “Gaussian-like” perturbations during training. Diffusion

models assume that the inputs are images corrupted by independent Gaussian noise  $\epsilon$ , as discussed in Equation (2). However, this assumption limits our ability to adjust  $\epsilon$  to enhance model robustness. To overcome this limitation, we advocate relaxing the independence assumption by introducing a modified noise term  $\epsilon'$ . Although  $\epsilon'$  follows a Gaussian distribution,  $\epsilon' \sim \mathcal{N}(0, \mathbf{I})$ , we allow its conditional distribution given  $\mathbf{x}$ , denoted  $\epsilon'|\mathbf{x}$ , to approximate a Gaussian distribution in a more flexible way,  $\epsilon'|\mathbf{x} \sim \mathcal{N}(0, \mathbf{I})$ . This allows us to design perturbations for each  $\mathbf{x}$ , while still adhering closely to the assumptions of the diffusion process.

To make the perturbations follow a Gaussian distribution, we use Rank-Based Gaussian Mapping (RBGM), as shown in Figure 5. We label RBGM as  $\epsilon_\delta(\cdot)$  and its input as  $\delta$ . RBGM trims  $\delta$  to fit Gaussian distribution, while preserving the original order of magnitude of its elements. RBGM could be illustrated as follows. We sample a Gaussian tensor  $\epsilon_s$  that matches the size of  $\delta$ . After ranking the elements of  $\delta$  and  $\epsilon_s$ , we replace the elements of  $\delta$  with the corresponding rank elements of  $\epsilon_s$ . Thus, if the rank of each element in  $\delta$  is uniformly distributed, then  $\epsilon_\delta(\delta)$  will follow  $\epsilon_\delta(\delta) \sim \mathcal{N}(0, \mathbf{I})$ . Although RBGM-mapped perturbations don’t satisfy  $\epsilon_\delta(\delta)|\mathbf{x} \sim \mathcal{N}(0, \mathbf{I})$ , the Gaussian distribution of  $\epsilon_\delta(\delta)$  allows us to blend it with random Gaussian noise to meet this condition. By merging RBGM-mapped perturbation and Gaussian noise, we can formulate the resulting  $\mathbf{x}'_t$  as follows:

$$\begin{aligned} \mathbf{x}'_t(\mathbf{x}_0, \epsilon, \epsilon_\delta(\delta)) &= \sqrt{\bar{\alpha}_t}\mathbf{x}_0 + \sqrt{1 - \lambda_t^2}\sqrt{1 - \bar{\alpha}_t}\epsilon \\ &\quad + \lambda_t\sqrt{1 - \bar{\alpha}_t}\epsilon_\delta(\delta) \end{aligned} \quad (6)$$

Here  $\lambda_t$  controls the amount of adversarial perturbations, this ensures that the total noise will still largely independent to  $\mathbf{x}_0$ , it also ensures that the perturbation are not too overwhelming for the denoising model to learn. We set  $\lambda_t$  as:

$$\lambda_t = \text{clip}(\gamma_t\lambda_{unit}, \lambda_{min}, \lambda_{max}) \quad \gamma_t = \frac{\sqrt{\bar{\alpha}_t}}{\sqrt{1 - \bar{\alpha}_t}} \quad (7)$$

where the clip function limits  $\lambda_t$  between  $\lambda_{min}$  and  $\lambda_{max}$ .

### 5.2. Adversarial Denoising Diffusion Training

**Training Step.** The training step is shown to the left of Figure 4. The goal of model optimization is to subtract the Gaussian noise and the RBGM-mapped perturbations to fully recover the image, this could be denoted as:

$$\theta^* = \arg \min_{\theta} \mathbb{E} \left[ \frac{\sqrt{\bar{\alpha}_t}}{\sqrt{1 - \bar{\alpha}_t}} \|\mathbf{x}_0 - \mathbf{P}(\mathbf{x}'_t, t)\|_2^2 \right] \quad (8)$$

where the expectation is taken with respect to  $\mathbf{x}_0 \sim \mathcal{D}$ ,  $t \sim \mathcal{U}(\{1, \dots, T\})$ ,  $\epsilon \sim \mathcal{N}(0, \mathbf{I})$ . The noise mixture  $\mathbf{x}'_t$  is derived from  $\mathbf{x}_0$ ,  $\epsilon$ , and  $\delta$  according to Equation (6),  $\mathbf{P}$  is

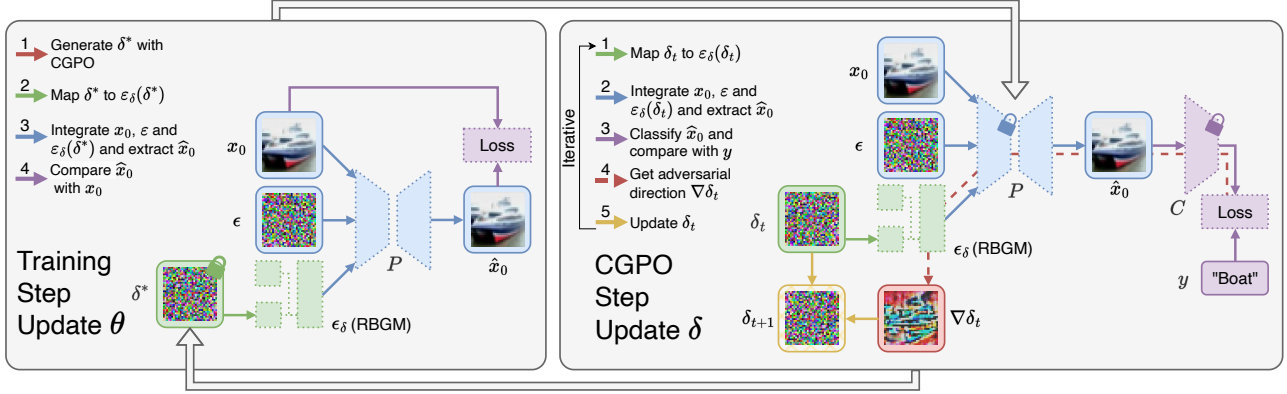


Figure 4: Adversarial Denoising Diffusion Training. In the CGPO step (right), perturbations are generated with classifier guidance. In the training step (left), the model trains with the generated perturbation. RBGM is used to make the perturbation compatible with diffusion models.

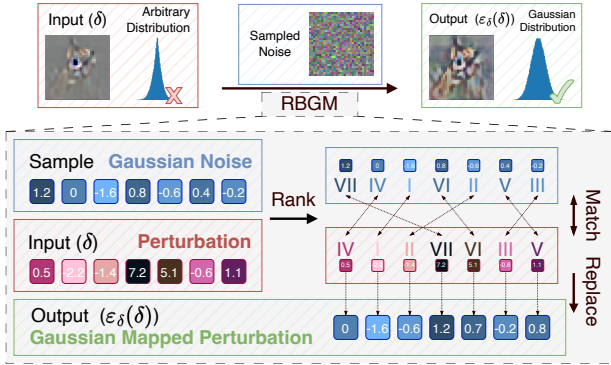


Figure 5: Rank-Based Gaussian Mapping. We first sample a Gaussian noise tensor that matches the size of the input tensor, rank the elements in each tensor, and replace the elements in the input tensor with elements in the Gaussian noise of the same rank.

the diffusion model, it takes  $x'_t$  and  $t$  to predict the original image  $\hat{x}_0$ . Note that in DDPM/DDIM the goal of the Unet is to predict the noise  $\epsilon$ , we use Equation (4) to transform the prediction to  $\hat{x}_0$ . Also note that since the DDPM/DDIM loss is the expectation of the noise distance, we add a factor  $\sqrt{\bar{\alpha}_t}/\sqrt{1-\bar{\alpha}_t}$  to keep our loss in line with the traditional DDPM/DDIM loss.

**CGPO Step.** The objective of generative models are distinct from those of downstream perceptual tasks. To generate perturbations that are meaningful for these tasks, we propose the incorporation of classifier guidance into the generation of perturbations with **Classifier-Guided Perturbation Optimization (CGPO)**<sup>3</sup>. As shown on the right side of Figure 4, we first reconstruct a clean image  $\hat{x}_0$  from  $x'_t$  with the diffu-

<sup>3</sup>Here we use the classifier only for semantic guidance, the classifier in CGPO doesn't need to be consistent with the protected model, see Section 6.3.

sion model  $P$ , we then classify the image with a pre-trained classifier  $C$ . The goal of CGPO is to refine the perturbation to maximize the classification error:

$$\delta^* = \arg \max_{\delta} \mathbb{E} [L(C(P(\theta, x'_t(x_0, \epsilon, \epsilon_\delta(\delta)), t)), y)] \quad (9)$$

To optimize  $\delta$ , we employ an iterative process of gradient accumulation, detailed in Appendix E. Given the non-differentiable nature of RBGM, we accumulate gradients with respect to  $\nabla_{\epsilon_\delta(\delta)}$  rather than  $\nabla_{\delta}$ . This is sufficient for training. In RBGM, we process each channel of every image independently. The distribution of the ranks of  $\delta$  elements, as analyzed in Appendix D, approximates a uniform distribution.

## 6. Experiments

### 6.1. Experiment Setup

**Classifier.** We train a WideResNet-28-10 classifier for 200 epochs following the methods in (Yoon et al., 2021; Wang et al., 2022) and achieve 95.12% accuracy on CIFAR-10 and 76.66% on CIFAR-100 dataset.

**DBP.** For DBP forward process timestep, DiffPure employs a continuous-time VPSDE (DDPM++) model, selecting  $t^* = 0.1$ . For discrete timesteps in Equation (2) of  $DP_{DDPM}$  and  $DP_{DDIM}$ , we set  $t^* = 0.1 \times T$ . For EDM models, we discuss the details in Appendix F.

**ADDT.** We fine-tune our diffusion model based on the CIFAR-10 pre-trained exponential moving average (EMA) clean model closely following its training setting (Ho et al., 2020) (transformed into Huggingface Diffusers format by (Fang et al., 2023)). The CIFAR-100 clean model is fine-tuned from the CIFAR-10 clean model for 100 epochs. ADDT models are fine-tuned from clean pre-trained models for 100 epochs, with guidance from the WideResNet-28-

Table 2: Clean and robust accuracy on CIFAR-10 obtained by different DBP methods. All methods show consistent improvement fine-tuned with ADDT.

Diffusion model	DBP model	Clean	$l_\infty$	$l_2$
-	-	95.12	0.00	1.46
DDIM	DP <sub>DDIM</sub>	88.38	42.19	70.02
	<b>DP<sub>DDIM</sub> Ours</b>	88.77	<b>46.48</b>	<b>71.19</b>
DDPM	GDMP (No Guided) (Wang et al., 2022)	91.41	40.82	69.63
	GDMP (MSE) (Wang et al., 2022)	91.80	40.97	70.02
	GDMP (SSIM) (Wang et al., 2022)	92.19	38.18	68.95
	DP <sub>DDPM</sub>	85.94	47.27	69.34
	<b>DP<sub>DDPM</sub> Ours</b>	85.64	<b>51.46</b>	<b>70.12</b>
DDPM++	COUP(Zhang et al., 2024)	90.33	50.78	71.19
	DiffPure	89.26	55.96	75.78
	<b>DiffPure Ours</b>	89.94	<b>62.11</b>	<b>76.66</b>
EDM	DP <sub>EDM</sub> (Appendix F)	86.43	62.50	76.86
	<b>DP<sub>EDM</sub> Ours(Appendix F)</b>	86.33	<b>66.41</b>	<b>79.16</b>

Table 3: Clean and robust accuracy on CIFAR-10, obtained by different classifiers. ADDT (WRN-28-10 guidance) Improved robustness in protecting different subsequent classifiers. (\*: the classifier used in ADDT fine-tuning).

Method	Classifier	Vanilla		Ours			
		Clean	$l_\infty$	$l_2$	Clean	$l_\infty$	$l_2$
DP <sub>DDPM-1000</sub>	VGG-16(Simonyan & Zisserman, 2014)	84.77	41.99	66.89	85.06	<b>46.09</b>	<b>67.87</b>
	ResNet-50(He et al., 2016)	83.11	44.04	67.58	83.84	<b>48.14</b>	<b>67.87</b>
	WRN-28-10*(Zagoruyko & Komodakis, 2016)	85.94	47.27	69.34	85.64	<b>51.46</b>	<b>70.12</b>
	WRN-70-16(Zagoruyko & Komodakis, 2016)	88.43	48.93	70.31	87.84	<b>52.54</b>	<b>70.70</b>
	ViT-B(Dosovitskiy et al., 2020)	85.45	45.61	69.53	85.25	<b>48.63</b>	<b>69.92</b>
DP <sub>DDIM-100</sub>	VGG-16(Simonyan & Zisserman, 2014)	87.16	29.00	61.82	87.55	<b>35.06</b>	<b>66.11</b>
	ResNet-50(He et al., 2016)	86.04	31.74	62.11	86.57	<b>38.77</b>	<b>65.82</b>
	WRN-28-10*(Zagoruyko & Komodakis, 2016)	88.96	43.16	67.58	88.18	<b>47.85</b>	<b>70.61</b>
	WRN-70-16(Zagoruyko & Komodakis, 2016)	84.40	39.16	68.36	84.96	<b>47.66</b>	<b>69.14</b>
	ViT-B(Dosovitskiy et al., 2020)	88.77	34.38	65.72	88.48	<b>41.02</b>	<b>68.65</b>
DP <sub>EDM</sub>	WRN-28-10*(Zagoruyko & Komodakis, 2016)	86.43	62.50	76.86	86.33	<b>66.41</b>	<b>79.16</b>
	WRN-70-16(Zagoruyko & Komodakis, 2016)	86.62	65.62	76.46	86.43	<b>69.63</b>	<b>78.91</b>

10 classifier. In CGPO we adopt  $\lambda_{unit} = 0.03$ ,  $\lambda_{min} = 0$ ,  $\lambda_{max} = 0.3$  and refine  $\delta$  for 5 iterations. Fine-tuning from clean models with ADDT is quite efficient, taking 12 hours on four NVIDIA GeForce RTX 2080ti GPUs for DDPM/DDIM models.

**Robustness Evaluation.** We adopt PGD20-EoT10 attack for robustness evaluation. For  $l_\infty$  attacks we set  $\alpha = 2/255$  and  $\epsilon = 8/255$ ; for  $l_2$  attacks we set  $\alpha = 0.1$  and  $\epsilon = 0.5$ . Due to computational constraints, we test the first 1024 images from the CIFAR-10/100 datasets. Note that it still takes 5 hours on four NVIDIA GeForce RTX 2080ti GPUs to test DDPM  $S = 1000$ .

## 6.2. Comparison with State-of-the-Art Approaches

We implemented ADDT fine-tuning across a range of diffusion models. We employ a DiffPure-style DBP approach with the fine-tuned models, and compare their performance with state-of-the-art DBP methods on the CIFAR-10 dataset. The outcomes, detailed in Table 2, reveal that ADDT fine-tuning enhances the robustness of these models, enabling them to reach state-of-the-art performance levels.

Table 4: Clean and robust accuracy on DP<sub>DDPM</sub>. ADDT improve robustness across different NFEs, especially at lower NFEs (\*: default DDPM generation setting, -: classifier only).

Dataset	NFE	Vanilla			Ours		
		Clean	$l_\infty$	$l_2$	Clean	$l_\infty$	$l_2$
CIFAR-10	-	95.12	0.00	1.46	95.12	0.00	1.46
	5	49.51	21.78	36.13	59.96	<b>30.27</b>	<b>41.99</b>
	10	73.34	36.72	55.47	78.91	<b>43.07</b>	<b>62.97</b>
	20	81.45	45.21	65.23	83.89	<b>48.44</b>	<b>69.82</b>
	50	85.54	46.78	68.85	85.45	<b>50.20</b>	<b>69.04</b>
	100*	85.94	47.27	69.34	85.64	<b>51.46</b>	<b>70.12</b>
CIFAR-100	-	76.66	0.00	2.44	76.66	0.00	2.44
	5	17.29	3.71	9.28	21.78	<b>6.25</b>	<b>13.77</b>
	10	34.08	10.55	19.24	40.62	<b>14.55</b>	<b>27.25</b>
	20	48.05	17.68	30.66	53.32	<b>18.65</b>	<b>36.13</b>
	50	55.57	20.02	37.70	59.47	<b>22.75</b>	<b>40.72</b>
	100*	57.52	20.41	37.89	59.18	<b>23.73</b>	<b>41.70</b>

Table 5: Clean and robust accuracy on DP<sub>DDIM</sub>. ADDT improve robustness across different NFEs (\*: default DDIM generation setting, -: classifier only).

Dataset	NFE	Vanilla			Ours		
		Clean	$l_\infty$	$l_2$	Clean	$l_\infty$	$l_2$
CIFAR-10	-	95.12	0.00	1.46	95.12	0.00	1.46
	5	89.65	42.19	68.65	88.57	<b>47.27</b>	<b>70.61</b>
	10*	88.96	43.16	67.58	88.18	<b>47.85</b>	<b>70.61</b>
	20	87.89	41.70	69.24	88.67	<b>48.63</b>	<b>69.73</b>
	50	88.96	42.48	68.85	88.57	<b>46.68</b>	<b>69.24</b>
	100	88.38	42.19	70.02	88.77	<b>46.48</b>	<b>71.19</b>
CIFAR-100	-	76.66	0.00	2.44	76.66	0.00	2.44
	5	62.11	15.43	35.74	62.79	<b>17.58</b>	<b>38.87</b>
	10*	62.21	15.33	36.52	64.45	<b>20.02</b>	<b>39.26</b>
	20	63.67	15.62	37.89	65.23	<b>18.65</b>	<b>40.62</b>
	50	62.40	16.31	37.79	63.87	<b>19.14</b>	<b>39.94</b>
	100	63.28	15.23	36.62	66.02	<b>18.85</b>	<b>39.84</b>

## 6.3. Defense Performance in Extensive Scenarios

**Performance on Different Classifier.** We evaluate the cross model protection ability of ADDT fine-tuned models, as shown in Table 3. The results indicate that fine-tuning with WRN-28-10 guided ADDT could enhance the ability to protect different classifiers. Notably, using DP<sub>EDM</sub>, we achieved 69.63%  $l_\infty$  robust accuracy on a WRN-70-16 classifier. This demonstrates that our method, without classifier-specific fine-tuning, can achieve comparable results to state-of-the-art AT based models.

**Performance under acceleration.** To speed up the diffusion process by omitting intermediate steps (Nichol & Dhariwal, 2021; Song et al., 2020a), several approaches have been proposed. In this section, we evaluate the robustness of accelerated DBP models. We quantify the acceleration by the number of neural function evaluations (NFE), which represents the number of evaluations performed during DBP inference. During the DBP process, we fix  $t^* = 0.1 \times T$ . To facilitate the acceleration, we omit intermediate time steps. For example, with an NFE of 5, the time steps for the DBP backward process would be  $t = [100, 80, 60, 40, 20, 0]$ . The results are detailed in Table 4 and Table 5. Our method improves the robustness of both DP<sub>DDPM</sub> and DP<sub>DDIM</sub> models.

Table 6: Clean and robust accuracy on Tiny-ImageNet with WRN-28-10 classifier. ADDT improve DBP robustness on Tiny-ImageNet (-: classifier only).

Method	Vanilla			Ours		
	Clean	$l_\infty$	$l_2$	Clean	$l_\infty$	$l_2$
-	71.37	0.00	0.00	-	-	-
DP <sub>DDPM</sub> -1000	57.13	11.82	46.68	56.15	<b>13.57</b>	<b>48.54</b>
DP <sub>DDIM</sub> -100	60.35	4.79	39.75	<b>60.45</b>	<b>5.86</b>	<b>40.82</b>

Table 7: FID score of DDPM for CIFAR-10 fine-tuned to different perturbations (the lower the better). Fine-tuning with RBGM-mapped perturbations yields lower FID scores than  $l_\infty$  perturbations.

	Vanilla	Clean Fine-tune	Ours	Ours $l_\infty$
FID	3.196	3.500	5.190	13.608

Note that the performance of DP<sub>DDPM</sub> varies significantly between different NFEs. This may be due to the fact that DDPM introduces stochasticity (Gaussian noise) at each reverse step; with fewer reverse steps, it’s stochasticity decreases. Also, the generation capability of DDPM is sensitive to the skipping of intermediate steps.

**Performance on Tiny-ImageNet.** We test DBP robustness on Tiny-ImageNet dataset (Le & Yang, 2015), with training and evaluation settings following CIFAR-10. The result shows that ADDT improves robustness on Tiny-ImageNet dataset.

#### 6.4. Ablation Study and Analysis

**RBGM.** We compare the generative ability of diffusion models fine-tuned with RBGM-mapped and  $l_\infty$  perturbations by comparing their Fréchet Inception Distance (FID) scores, as shown in Table 7. The results showed that diffusion models fine-tuned with RBGM-mapped perturbations maintain generation quality comparable to the vanilla diffusion model, while models fine-tuned with  $l_\infty$  perturbations show degraded performance. We also observed that training with RBGM-mapped perturbations generalized better to different attacks. Experimental details and additional tests are presented in Appendix H.

**CGPO.** We examine the effect of vanilla fine-tuning and ADDT fine-tuning with MSE distance guidance (without classifier guidance) in Table 8. Neither method improves the robustness of DBP models.

**Revisiting DBP Robustness.** We re-examined robustness under the deterministic white-box setting by evaluating the performance of diffusion models after ADDT fine-tuning. The fine-tuned models showed significantly higher robustness under the Deterministic White-box setting, indicating that our method makes the attack more difficult without relying on the evasion effect of stochastic elements. We

Table 8: Clean and robust accuracy on CIFAR-10 fine-tuned to different methods. Vanilla fine-tuning and fine-tuning with non-classifier-guided perturbations did not improve robustness.

Method	NFE	Vanilla Fine-tune Only			MSE Distance Guided		
		Clean	$l_\infty$	$l_2$	Clean	$l_\infty$	$l_2$
DP <sub>DDPM</sub>	5	47.27	21.88	33.11	49.32	21.19	35.74
	10	71.58	34.77	52.64	73.34	36.43	55.96
	20	81.93	42.29	63.77	83.79	42.87	66.89
	50	84.18	47.56	65.53	85.16	47.27	67.87
	100*	85.25	47.27	68.26	86.91	46.97	70.80
DP <sub>DDIM</sub>	5	89.26	41.11	67.87	89.45	39.36	67.58
	10*	88.87	41.41	67.19	89.36	40.92	67.68
	20	89.45	40.23	67.77	88.48	42.68	68.55
	50	88.77	42.09	67.38	88.18	41.02	68.16
	100	88.18	40.62	68.26	89.26	40.33	68.36

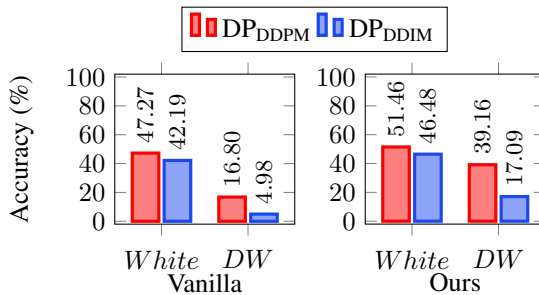


Figure 6: Revisiting Deterministic White-box setting. ADDT improved robustness under both White-box and Deterministic White-box setting, implying that ADDT strengthens the models’ ability to counter adversarial inputs.

provide a more detailed experiment considering different NFEs in Appendix J. We then compared the loss landscapes of ADDT fine-tuned models and vanilla diffusion models, as shown in Figure 3. This comparison showed that our method effectively smooths the loss landscape of DBP models.

## 7. Conclusion

In summary, We re-examined DBP robustness with a precise gradient, and discussed the impact of stochasticity. To better explain DBP robustness, we assessed DBP robustness under a novel attack setting, Deterministic White-box, pinpointing stochasticity as the key to DBP robustness. Our findings suggest diffusion models may rely on stochasticity to evade the most effective attack direction, rather than directly countering adversarial perturbations. To address this, we introduce **Adversarial Denoising Diffusion Training**, a novel approach that equips diffusion models with the ability to directly counter adversarial perturbations. Our empirical evaluations show that ADDT improves the robustness of diffusion models. Further experiments verify that ADDT gives the model the ability to directly counter adversarial perturbations.

## 8. Broader Impact

This paper presents work aimed at advancing the field of neural network robustness. Our work has many potential societal implications, whether in the realm of autonomous driving, facial recognition payment systems, medical assistance, etc. We are committed to improving the safety and trustworthiness of AI applications in the world.

## References

- Athalye, A., Carlini, N., and Wagner, D. Obfuscated gradients give a false sense of security: Circumventing defenses to adversarial examples. In *International conference on machine learning*, pp. 274–283. PMLR, 2018.
- Carlini, N., Tramer, F., Dvijotham, K. D., Rice, L., Sun, M., and Kolter, J. Z. (certified!!) adversarial robustness for free! In *The Eleventh International Conference on Learning Representations*, 2022.
- Chen, T., Xu, B., Zhang, C., and Guestrin, C. Training deep nets with sublinear memory cost. *arXiv preprint arXiv:1604.06174*, 2016.
- Croce, F. and Hein, M. Reliable evaluation of adversarial robustness with an ensemble of diverse parameter-free attacks. In *International conference on machine learning*, pp. 2206–2216. PMLR, 2020.
- Croce, F., Andriushchenko, M., Sehwag, V., Debenedetti, E., Flammarion, N., Chiang, M., Mittal, P., and Hein, M. Robustbench: a standardized adversarial robustness benchmark. *arXiv preprint arXiv:2010.09670*, 2020.
- Dosovitskiy, A., Beyer, L., Kolesnikov, A., Weissenborn, D., Zhai, X., Unterthiner, T., Dehghani, M., Minderer, M., Heigold, G., Gelly, S., et al. An image is worth 16x16 words: Transformers for image recognition at scale. *arXiv preprint arXiv:2010.11929*, 2020.
- Fang, G., Ma, X., and Wang, X. Structural pruning for diffusion models. *arXiv preprint arXiv:2305.10924*, 2023.
- Gao, Y., Shumailov, I., Fawaz, K., and Papernot, N. On the limitations of stochastic pre-processing defenses. *Advances in Neural Information Processing Systems*, 35: 24280–24294, 2022.
- Goodfellow, I. J., Shlens, J., and Szegedy, C. Explaining and harnessing adversarial examples. In Bengio, Y. and LeCun, Y. (eds.), *3rd International Conference on Learning Representations, ICLR 2015, San Diego, CA, USA, May 7-9, 2015, Conference Track Proceedings*, 2015. URL <http://arxiv.org/abs/1412.6572>.
- Gowal, S., Qin, C., Uesato, J., Mann, T. A., and Kohli, P. Uncovering the limits of adversarial training against norm-bounded adversarial examples. *CoRR*, abs/2010.03593, 2020. URL <https://arxiv.org/abs/2010.03593>.
- Gowal, S., Rebuffi, S.-A., Wiles, O., Stimberg, F., Calian, D. A., and Mann, T. A. Improving robustness using generated data. *Advances in Neural Information Processing Systems*, 34:4218–4233, 2021.
- He, K., Zhang, X., Ren, S., and Sun, J. Deep residual learning for image recognition. In *Proceedings of the IEEE conference on computer vision and pattern recognition*, pp. 770–778, 2016.
- Ho, J., Jain, A., and Abbeel, P. Denoising diffusion probabilistic models. *arXiv preprint arxiv:2006.11239*, 2020.
- Karras, T., Aittala, M., Aila, T., and Laine, S. Elucidating the design space of diffusion-based generative models. *Advances in Neural Information Processing Systems*, 35: 26565–26577, 2022.
- Kim, H., Lee, W., and Lee, J. Understanding catastrophic overfitting in single-step adversarial training. In *Proceedings of the AAAI Conference on Artificial Intelligence*, volume 35, pp. 8119–8127, 2021.
- Le, Y. and Yang, X. Tiny imagenet visual recognition challenge. *CS 231N*, 7(7):3, 2015.
- Li, H., Xu, Z., Taylor, G., Studer, C., and Goldstein, T. Visualizing the loss landscape of neural nets. *Advances in neural information processing systems*, 31, 2018.
- Madry, A., Makelov, A., Schmidt, L., Tsipras, D., and Vladu, A. Towards deep learning models resistant to adversarial attacks. In *6th International Conference on Learning Representations, ICLR 2018, Vancouver, BC, Canada, April 30 - May 3, 2018, Conference Track Proceedings*. OpenReview.net, 2018. URL <https://openreview.net/forum?id=rJzIBfZAb>.
- Nichol, A. Q. and Dhariwal, P. Improved denoising diffusion probabilistic models. In *International Conference on Machine Learning*, pp. 8162–8171. PMLR, 2021.
- Nie, W., Guo, B., Huang, Y., Xiao, C., Vahdat, A., and Anandkumar, A. Diffusion models for adversarial purification. In *International Conference on Machine Learning (ICML)*, 2022.
- OpenAI. Gpt-4 technical report. *ArXiv*, abs/2303.08774, 2023. URL <https://api.semanticscholar.org/CorpusID:257532815>.

- Radford, A., Kim, J. W., Xu, T., Brockman, G., McLeavey, C., and Sutskever, I. Robust speech recognition via large-scale weak supervision. *ArXiv*, abs/2212.04356, 2022. URL <https://api.semanticscholar.org/CorpusID:252923993>.
- Rebuffi, S.-A., Gowal, S., Calian, D. A., Stimberg, F., Wiles, O., and Mann, T. A. Fixing data augmentation to improve adversarial robustness. *ArXiv*, abs/2103.01946, 2021. URL <https://api.semanticscholar.org/CorpusID:232092181>.
- Samangouei, P., Kabkab, M., and Chellappa, R. Defensegan: Protecting classifiers against adversarial attacks using generative models. *arXiv preprint arXiv:1805.06605*, 2018.
- Shafahi, A., Najibi, M., Ghiasi, A., Xu, Z., Dickerson, J. P., Studer, C., Davis, L. S., Taylor, G., and Goldstein, T. Adversarial training for free! In *Neural Information Processing Systems*, 2019. URL <https://api.semanticscholar.org/CorpusID:139102395>.
- Simonyan, K. and Zisserman, A. Very deep convolutional networks for large-scale image recognition. *arXiv preprint arXiv:1409.1556*, 2014.
- Song, J., Meng, C., and Ermon, S. Denoising diffusion implicit models. *arXiv:2010.02502*, October 2020a. URL <https://arxiv.org/abs/2010.02502>.
- Song, Y. and Ermon, S. Generative modeling by estimating gradients of the data distribution. *Advances in neural information processing systems*, 32, 2019.
- Song, Y., Kim, T., Nowozin, S., Ermon, S., and Kushman, N. Pixeldefend: Leveraging generative models to understand and defend against adversarial examples. In *International Conference on Learning Representations*, 2018. URL <https://openreview.net/forum?id=rJUYGxbCW>.
- Song, Y., Sohl-Dickstein, J., Kingma, D. P., Kumar, A., Ermon, S., and Poole, B. Score-based generative modeling through stochastic differential equations. *arXiv preprint arXiv:2011.13456*, 2020b.
- Song, Y., Sohl-Dickstein, J., Kingma, D. P., Kumar, A., Ermon, S., and Poole, B. Score-based generative modeling through stochastic differential equations. In *International Conference on Learning Representations*, 2021. URL <https://openreview.net/forum?id=PxtTIG12RRHS>.
- Szegedy, C., Zaremba, W., Sutskever, I., Bruna, J., Erhan, D., Goodfellow, I. J., and Fergus, R. Intriguing properties of neural networks. In Bengio, Y. and LeCun, Y. (eds.), *2nd International Conference on Learning Representations, ICLR 2014, Banff, AB, Canada, April 14-16, 2014, Conference Track Proceedings*, 2014. URL <http://arxiv.org/abs/1312.6199>.
- Wang, J., Lyu, Z., Lin, D., Dai, B., and Fu, H. Guided diffusion model for adversarial purification. *arXiv preprint arXiv:2205.14969*, 2022.
- Wang, Z., Pang, T., Du, C., Lin, M., Liu, W., and Yan, S. Better diffusion models further improve adversarial training. In *International Conference on Machine Learning (ICML)*, 2023.
- Wu, Q., Ye, H., and Gu, Y. Guided diffusion model for adversarial purification from random noise. *arXiv preprint arXiv:2206.10875*, 2022.
- Xiao, C., Chen, Z., Jin, K., Wang, J., Nie, W., Liu, M., Anandkumar, A., Li, B., and Song, D. Densepure: Understanding diffusion models towards adversarial robustness. *arXiv preprint arXiv:2211.00322*, 2022.
- Yoon, J., Hwang, S. J., and Lee, J. Adversarial purification with score-based generative models. In *International Conference on Machine Learning*, pp. 12062–12072. PMLR, 2021.
- Zagoruyko, S. and Komodakis, N. Wide residual networks. *arXiv preprint arXiv:1605.07146*, 2016.
- Zhang, H., Yu, Y., Jiao, J., Xing, E. P., Ghaoui, L. E., and Jordan, M. I. Theoretically principled trade-off between robustness and accuracy. In *International Conference on Machine Learning*, 2019.
- Zhang, M., Li, J., Chen, W., Guo, J., and Cheng, X. Classifier guidance enhances diffusion-based adversarial purification by preserving predictive information, 2024. URL <https://openreview.net/forum?id=qvLPTx52ZR>.

## A. Influence of EoT Iterations on DBP Robustness Evaluation

In this section, we examine how the number of EoT iterations influences the DBP robustness evaluation. As previously discussed in Section 4.2, the Deterministic White-box attack could find the most effective attack direction. To quantify the impact of EoT iterations, we compare the attack direction of the standard White-box (EoT) across various numbers of EoT iterations with that of the Deterministic White-box.

See Figure 7 for a visual explanation, where the red line shows the DBP accuracy after attack, and the blue line shows the similarity between the attack directions of the White-box (EoT) and Deterministic White-box. The trend is clear: more EoT iterations lead to greater similarity and lower model accuracy, the rate of increase in similarity and the rate of decrease in accuracy both tend to slow down with further iterations.

Balancing computational cost and evaluation accuracy, we chose the PGD20-EoT10 configuration for our robustness evaluation.

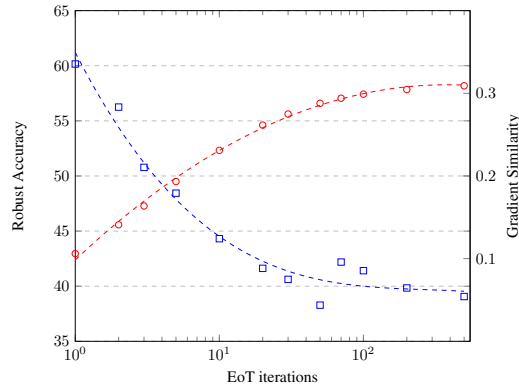


Figure 7: Robust accuracy and gradient similarity on  $DP_{DDPM}$  for CIFAR-10, obtained by different EoT iterations. As the number of EoT iterations increases, the gradient similarity between the White-box (EoT) attack direction and the Deterministic White-box attack direction increases and the robust accuracy decreases.

## B. All Noise Settings Cannot be Attacked All at Once

Building on the concept of Deterministic White-box, we propose  $DW_{semi-128}$ . Unlike Deterministic White-box, which attacks a DBP model under a single set of stochastic noise,  $DW_{semi-128}$  simultaneously attacks over 128 different sets of noise. It uses the average adversarial direction from these 128 noise settings (EoT-128) to perturb the DBP model. To understand the impact of stochasticity, we analyze the changes in the model’s loss under DW-box attack and  $DW_{semi-128}$  attack. We plot these changes by adjusting a factor  $k$  to modify an image  $x$  with a perturbation  $\sigma$ , evaluating the loss at  $x + k\sigma$  with  $k$  varying from  $-16$  to  $16$ . We generate perturbations with  $l_\infty$  Fast Gradient Sign Method (FGSM) (Goodfellow et al., 2015) with magnitude  $1/255$ . The plot is evaluated using WideResNet-28-10 with  $DP_{DDPM}$  over the first 128 images of CIFAR-10 dataset.

As Figure 8 shows, in the Deterministic White-box setting, the perturbations significantly increased the loss, proving their effectiveness. However, for  $DW_{semi-128}$ , where the attack spans multiple noise setting, the increase in loss is more moderate. This suggests that even when the attackers are fully informed about the stochastic noise choices, stochasticity still improves the robustness of the DBP. This challenging the notion that there exists a vulnerable direction effective across for all stochastic noise.

## C. Experimental Setting of Visualization of the Attack Trajectory

We visualize the attack by plotting the loss landscape and trace the trajectories of EoT attack under White-box setting and the Deterministic White-box setting in Figure 3. We run a vanilla PGD20-EoT10 attack under White-box setting and a PGD20 attack under Deterministic White-box setting. We then expand a 2D space using the final perturbations from these two attacks, draw the loss landscape, and plot the attack trajectories on it. Note that the two adversarial perturbation

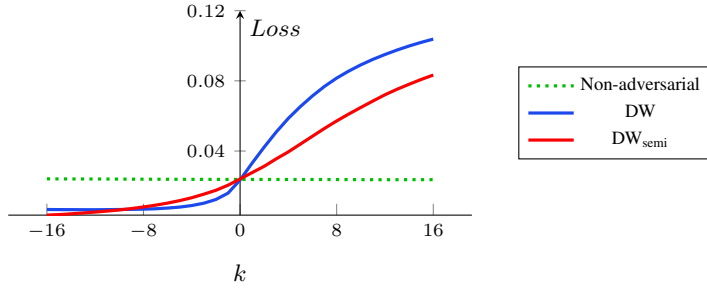


Figure 8: Impact of stochasticity on perturbation efficacy. Perturbations created under  $DW_{\text{semi}}$ -box setting are less potent compared to  $DW$ -box setting. For non-adversarial perturbations, we randomly assign each element a value of either  $1/255$  or  $-1/255$ .

directions are not strictly orthogonal. To extend this 2D space, we use the Deterministic White-box attack direction and the orthogonal component of the EoT attack direction. Note that the endpoints of both trajectories lie exactly on the loss landscape, while intermediate points are projected onto it. The plot is evaluated using WideResNet-28-10 with  $DP_{\text{DDPM}}$  over the first 128 images of CIFAR-10 dataset.

#### D. Rank Distribution of adversarial perturbation

The rank distribution of the accumulated gradient, as shown in Figure 9, approximately follows a uniform distribution.

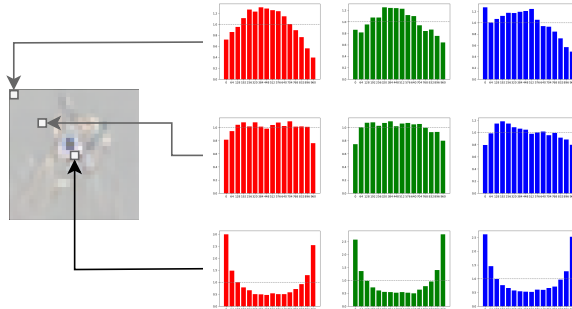


Figure 9: Histogram of  $\delta$  rank: We present a histogram for the R, G, B channels of pixels at positions  $[1,1]$ ,  $[8,8]$ , and  $[16,16]$  over a  $32 \times 32$  pixel grid. The rank distribution for these pixels approximately follows a uniform distribution from 1 to 1024 ( $32 \times 32$ ).

#### E. Pseudo-code of ADDT

The pseudo-code for adopting ADDT within DDPM and DDIM framework is shown in Algorithm 1.

#### F. Adopting VPSDE(DDPM++) and EDM Models in DBP

In Section 4.2, we mainly evaluate the robustness of DBP methods based on DDPM and DDIM models. We here also extend the analysis to VPSDE(DDPM++) and EDM framework (Karras et al., 2022). VPSDE(DDPM++) is the generative method used in DiffPure.

From a unified perspective, diffusion processes can be modeled as Stochastic Differential Equations (SDEs) (Song et al., 2021). The forward process of SDEs in Equation (10) progressively transforms a complex data distribution into a known prior by gradually adding noise, it could also be achieved in one step in Equation (11) like DDPM in Equation (2). While the

---

**Algorithm 1** Adversarial Denoising Diffusion Training (ADDT)

---

**Require:**  $\mathbf{x}_0$  is image from training dataset,  $y$  is the class label of the image,  $C$  is the classifier,  $P$  is one-step diffusion reverse process and  $\theta$  is its parameter,  $L$  is CrossEntropy Loss.

```

1: for  $\mathbf{x}_0, y$  in the training dataset do
2:    $t \sim \text{Uniform}(\{1, \dots, T\})$ 
3:    $\lambda_t = \text{clip}(\gamma_t \lambda_{\text{unit}}, \lambda_{\text{min}}, \lambda_{\text{max}})$ , where  $\gamma_t = \frac{\sqrt{\alpha_t}}{\sqrt{1-\alpha_t}}$ 
4:   Init  $\delta$  to a small random vector.
5:   for 1 to  $\text{ADDT}_{\text{iterations}}$  do
6:      $\epsilon \sim \mathcal{N}(0, I)$ 
7:      $\epsilon_\delta = \text{RBGM}(\delta)$ 
8:      $\mathbf{x}_t = \sqrt{\alpha_t} \mathbf{x}_0 + \sqrt{1-\lambda_t^2} \sqrt{1-\alpha_t} \epsilon + \lambda_t \sqrt{1-\alpha_t} \epsilon_\delta$ 
9:      $\delta = \delta + \nabla_{\epsilon_\delta} L(C(P(\mathbf{x}_t, t), y))$ 
10:   end for
11:    $\epsilon \sim \mathcal{N}(0, I)$ 
12:    $\epsilon_\delta = \text{RBGM}(\delta)$ 
13:    $\mathbf{x}_t = \sqrt{\alpha_t} \mathbf{x}_0 + \sqrt{1-\lambda_t^2} \sqrt{1-\alpha_t} \epsilon + \lambda_t \sqrt{1-\alpha_t} \epsilon_\delta$ 
14:   Take a gradient descent step on:
      $\nabla_{\theta} \left\| \frac{\sqrt{\alpha_t}}{\sqrt{1-\alpha_t}} (\mathbf{x}_0 - P(\mathbf{x}_t, t)) \right\|_2^2$ 
15: end for

```

Diffusion model  $\epsilon_\theta$  predicts the Gaussian noise added to the image, adopting Equation (4) in the paper, we have  $P(\mathbf{x}_t, t) = (\mathbf{x}_t - \sqrt{1-\alpha_t} \epsilon_\theta(\mathbf{x}_t, t)) / \sqrt{\alpha_t}$

---

reverse process Equation (12) of SDEs, gradually restores this prior distribution to the original data distribution.

$$d\mathbf{x} = \mathbf{f}(\mathbf{x}, t)dt + g(t)d\mathbf{w} \quad (10)$$

$$p_{0t}(\mathbf{x}(t) | \mathbf{x}(0)) = \mathcal{N}\left(\mathbf{x}(t); e^{-\frac{1}{4}t^2(\bar{\beta}_{\text{max}}-\bar{\beta}_{\text{min}})-\frac{1}{2}t\bar{\beta}_{\text{min}}}\mathbf{x}(0), \mathbf{I} - \mathbf{I}e^{-\frac{1}{2}t^2(\bar{\beta}_{\text{max}}-\bar{\beta}_{\text{min}})-t\bar{\beta}_{\text{min}}}\right), \quad t \in [0, 1] \quad (11)$$

$$d\mathbf{x} = \left[\mathbf{f}(\mathbf{x}, t) - g^2(t)\nabla_{\mathbf{x}} \log p_t(\mathbf{x})\right] dt + g(t)d\bar{\mathbf{w}} \quad (12)$$

The reverse process of SDEs also derives equivalent ODEs Equation (13) for fast sampling and exact likelihood computation, and this Score ODEs corresponds to DDIM.

$$d\mathbf{x} = \left[\mathbf{f}(\mathbf{x}, t) - \frac{1}{2}g(t)^2\nabla_{\mathbf{x}} \log p_t(\mathbf{x})\right] dt \quad (13)$$

By adjusting the level of stochasticity, we are able to generate a wide range of semi-stochastic models that interpolated between pure SDEs and ODEs with varying degrees of stochasticity.

We also try to adopt diffusion models like EDM to further improve DBP robustness. EDM present a design space that distinctly separates the concrete design choices from the unnecessarily convoluted theory and practice of diffusion-based generative models (DDPM, DDIM, iDDPM (Nichol & Dhariwal, 2021), VPSDE, VESDE (Song et al., 2021)). The adaptations to both the sampling and training procedures (Heun sampler,  $\sigma(t)$ ,  $s(t)$ ), in conjunction with the preconditioning of the score networks, enable it to achieve state-of-the-art performance in generative tasks.

EDM forward process could be presented as:

$$\mathbf{x}_t = \mathbf{x}_0 + \sigma(t^*) * \epsilon, \quad \epsilon \sim \mathcal{N}(0, \mathbf{I}) \quad (14)$$

where we choose  $\sigma(t^*) = 0.5$  for clean and robust accuracy tradeoff. And for reverse process, EDM incorporates a parameter  $S_{\text{churn}}$  to modulate the stochastic noise infused during the reverse process. For our experiments, we choose 50 reverse steps (50 NFEs, NFEs is Function of Neural Function Evaluations), configured the parameters with  $S_{\text{min}} = 0.01$ ,  $S_{\text{max}} = 0.46$ ,  $S_{\text{noise}} = 1.007$ , and designate  $S_{\text{churn}} = 0$  to represent EDM-ODE,  $S_{\text{churn}} = 6$  to represent EDM-SDE.

As shown in Table 9, our ADDT could also increase the robustness of  $\text{DP}_{\text{EDM}}$ .

## G. Strengthening DBP via Augmented Stochasticity

Song et al. present a Predictor-Corrector sampler for SDEs reverse process for VPSDE (DDPM++) (as detailed in Appendix G of (Song et al., 2021)). However, standard implementations of VPSDE (DDPM++) typically use only the Predictor. Given

Table 9: Clean and robust accuracy on  $DP_{EDM}$  for CIFAR-10. ADDT improves robustness in both  $DP_{EDM-SDE}$  and  $DP_{EDM-ODE}$ .

Type	Vanilla		Ours	
	$DP_{EDM-SDE}$	$DP_{EDM-ODE}$	$DP_{EDM-SDE}$	$DP_{EDM-ODE}$
Clean	<b>86.43</b>	<b>87.99</b>	86.33	<b>87.99</b>
$l_\infty$	62.50	60.45	<b>66.41</b>	<b>64.16</b>
$l_2$	76.86	75.49	<b>79.16</b>	<b>77.15</b>

Table 10: Clean and robust accuracy on  $DP_{DDPM++}$  for CIFAR-10. Both extra Corrector and ADDT fine-tuning improved robustness.

Type	Vanilla	Extra Corrector	ADDT	ADDT+Extra Corrector
Clean	89.26	85.25	<b>89.94</b>	85.55
$l_\infty$	55.96	59.77	62.11	<b>65.23</b>
$l_2$	75.78	74.22	<b>76.66</b>	<b>76.66</b>

our hypothesis that stochasticity contributes to robustness, we expect that integrating the Corrector sampler into VPSDE (DDPM++) would further enhance the robustness of DBP models. Our empirical results, as shown in Table 10, confirm that the inclusion of a Corrector to VPSDE (DDPM++) indeed improve the model’s defenses ability against adversarial attacks with  $l_\infty$  norm constraints. This finding supports our claim that the increased stochasticity can further strengthen DBP robustness. Adding Corrector is also consistent with ADDT. Note that the robustness against  $l_2$  norm attacks does not show a significant improvement with the integration of the Extra Corrector. A plausible explanation for this could be that the performance under  $l_2$  attacks is already quite strong, and the compromised performance on clean data counteracted the increase in robustness.

## H. Evaluating RBGM-Mapped Perturbations

In Section 6.4, we briefly explored the generation capabilities of diffusion models trained with RBGM-mapped and  $l_\infty$  perturbations. Here, we provide details of the experiment and delve deeper into their robustness. To train with  $l_\infty$  perturbations, we adjusted ADDT, replacing RBGM-mapped perturbations with  $l_\infty$  perturbations. Here, instead of converting accumulated gradients to Gaussian-like perturbations, we used a 5-step projected gradient descent (PGD-5) approach. We also set  $\lambda_{unit} = 1$ ,  $\lambda_{min} = 0$ ,  $\lambda_{max} = 10$ . We refer to this modified training protocol as  $ADDT_{l_\infty}$ .

Table 11: Clean and robust accuracy on DBP models trained with different perturbations for CIFAR-10. While ADDT simultaneously improves clean accuracy and robustness against both  $l_2$  and  $l_\infty$  attacks.  $ADDT_{l_\infty}$  primarily improves performance against  $l_\infty$  attacks.

Method	Dataset	Vanilla			ADDT			$ADDT_{l_\infty}$		
		Clean	$l_\infty$	$l_2$	Clean	$l_\infty$	$l_2$	Clean	$l_\infty$	$l_2$
$DP_{DDPM-1000}$	CIFAR-10	<b>85.94</b>	47.27	69.34	85.64	51.46	<b>70.12</b>	84.47	<b>52.64</b>	68.55
	CIFAR-100	57.52	20.41	37.89	<b>59.18</b>	<b>23.73</b>	<b>41.70</b>	57.81	23.24	40.04
$DP_{DDIM-100}$	CIFAR-10	88.38	42.19	70.02	<b>88.77</b>	46.48	<b>71.19</b>	88.48	<b>50.49</b>	70.31
	CIFAR-100	63.28	15.23	36.62	<b>66.02</b>	18.85	<b>39.84</b>	64.84	<b>20.31</b>	39.36

We evaluated the clean and robust accuracy of ADDT and  $ADDT_{l_\infty}$  fine-tuned models. These models exhibited different behaviors. As shown in Table 11, while Gaussian-mapped perturbations can simultaneously improve clean accuracy and robustness against both  $l_2$  and  $l_\infty$  attacks, training with  $l_\infty$  perturbations primarily improves performance against  $l_\infty$  attacks.

Table 12: AutoAttack (*Rand* version) and PGD20-EoT10 performance on DBP methods for CIFAR-10 (the lower the better). The original AutoAttack produced high accuracy, after fix, it achieved similar results to PGD20+EoT10 attack.

Method	$l_\infty$			$l_2$		
	AutoAttack	AutoAttack <sub>Ours</sub>	PGD20-EoT10	AutoAttack	AutoAttack <sub>Ours</sub>	PGD20-EoT10
DiffPure	62.11	56.25	<b>55.96</b>	81.84	76.37	<b>75.78</b>
DP <sub>DDPM-1000</sub>	57.81	<b>46.88</b>	48.63	71.68	<b>71.09</b>	72.27
DP <sub>DDIM-100</sub>	50.20	<b>40.62</b>	44.73	77.15	<b>70.70</b>	71.68

Table 13: Clean and robust accuracy on different DBP methods for CIFAR-10, evaluated with AutoAttack<sub>Ours</sub> (*Rand* version). All methods showed consistent improvement when fine-tuned with ADDT.

Method	Vanilla			Ours		
	<i>Clean</i>	$l_\infty$	$l_2$	<i>Clean</i>	$l_\infty$	$l_2$
DiffPure	89.26	56.25	76.37	<b>89.94</b>	<b>58.20</b>	<b>77.34</b>
DP <sub>DDPM</sub>	<b>85.94</b>	46.88	71.09	85.64	<b>48.63</b>	<b>72.27</b>
DP <sub>DDIM</sub>	88.38	40.62	70.70	<b>88.77</b>	<b>44.73</b>	<b>71.68</b>

## I. Evaluating under Fixed AutoAttack

AutoAttack (Croce & Hein, 2020), an ensemble of White-box and Black-box attacks, is a popular benchmark for evaluating model robustness. It is used in RobustBench (Croce et al., 2020) to evaluate over 120 models. However, Nie et al. (Nie et al., 2022) found that the *Rand* version of AutoAttack, designed to evaluate stochastic defenses, sometimes yields higher accuracy than the *Standard* version, intended for deterministic methods. Our comparison of AutoAttack and PGD20-EoT10 in Table 12 also showed that the *Rand* version of AutoAttack gives higher accuracy than the PGD20-EoT10 attack.

We attribute this to the sample selection of AutoAttack. As an ensemble of attack methods, AutoAttack selects the final adversarial sample from either the original input or the attack results. However, the original implementation neglects stochasticity and considers a adversarial sample to be sufficiently adversarial if it gives a false result in one evaluation. To fix this, we propose a 20-iteration evaluation and selects the adversarial example with the lowest accuracy. The flawed code is in the official GitHub main branch, git version `a39220048b3c9f2cca9a4d3a54604793c68eca7e`, and specifically in lines #125, #129, #133-136, #157, #221-225, #227-228, #231 of the file `autoattack/autoattack.py`. We will open source our updated code and encourage future stochastic defense methods to be evaluated against the fixed code. The code can be found at: <https://anonymous.4open.science/r/auto-attack-595C/README.md>.

After the fix, AutoAttack’s accuracy dropped by up to 10 points, producing similar results to our PGD20-EoT10 test results. However, using AutoAttack on DP<sub>DDPM</sub> with  $S = 1000$  took nearly 25 hours, five times longer than PGD20-EoT10, so we will use PGD20-EoT10 for the following test.

## J. Robustness under Deterministic White-box Setting

We evaluated robustness of ADDT fine-tuned models under Deterministic White-box Setting. We assessed robustness across varying NFEs and compared the performance of vanilla models and ADDT fine-tuned models, with results showcased in Figure 10. ADDT consistently improved model performance at different NFEs, particularly noticeable at lower NFEs. This affirms that ADDT equips the diffusion model with the ability to directly counter adversarial perturbations.

## K. Computational Cost of ADDT

Optimizing DDPM and DDIM models through ADDT achieves near-optimal performance in 50 epochs. This process takes only 12 hours on a four-GPU cluster of NVIDIA GeForce RTX 2080 Ti, matching the speed of traditional adversarial training and significantly faster than the latest adversarial training techniques that use diffusion models to augment the dataset (Wang et al., 2023).

A special feature of ADDT is its one-and-done training approach. After initial training, ADDT can protect various classifiers

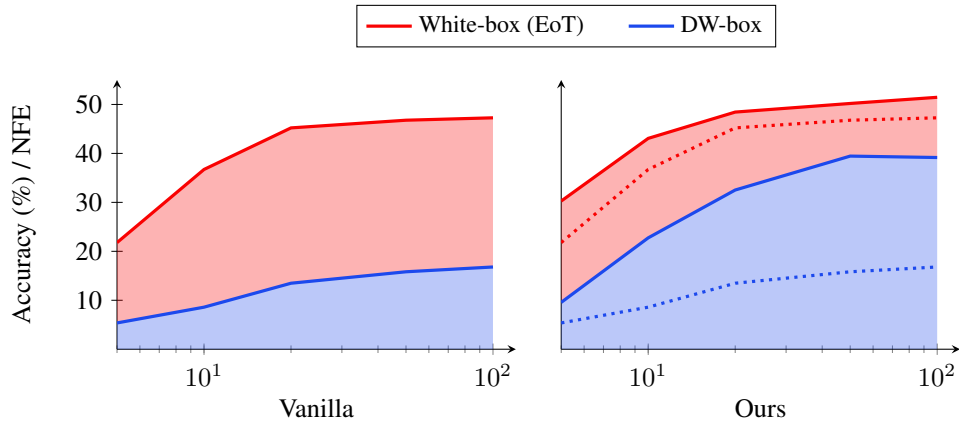


Figure 10: Revisiting Deterministic White-box Robustness. ADDT improved robustness under both white box and Deterministic White-box setting, implying that ADDT strengthens the models’ ability to handle adversarial inputs. The dashed line on the right is the performance of the vanilla model.

without the need for further fine-tuning, as shown in Table 3. This is different from adversarial classifier training, which requires individual training for each classifier.

## L. Credibility of Our Paper

The code was developed independently by two individuals and mutually verified, with consistent results achieved through independent training and testing. We will also make the code open-source and remain committed to advancing the field.